Large-eddy simulation of flows past a flapping airfoil using immersed boundary method[†]

YANG XiaoLei, HE GuoWei[*] & ZHANG Xing

The State Key Laboratory of Nonlinear Mechanics, Institute of Mechanics, Chinese Academy of Sciences, Beijing 100190, China

The numerical simulation of flows past flapping foils at moderate Reynolds numbers presents two challenges to computational fluid dynamics: turbulent flows and moving boundaries. The direct forcing immersed boundary (IB) method has been developed to simulate laminar flows. However, its performance in simulating turbulent flows and transitional flows with moving boundaries has not been fully evaluated. In the present work, we use the IB method to simulate fully developed turbulent channel flows and transitional flows past a stationary/plunging SD7003 airfoil. To suppress the non-physical force oscillations in the plunging case, we use the smoothed discrete delta function for interpolation in the IB method. The results of the present work demonstrate that the IB method can be used to simulate turbulent flows and transitional flows with moving boundaries.

transitional flows, moving boundary, immersed boundary method, smoothed discrete delta function

PACS: 47.85.Gj, 47.11.Df, 47.27.Cn

1   Introduction

The fluid dynamics of transitional flows past airfoils at Reynolds number 10^4 to 10^5 receives attention recently with the development in small-sized air vehicles, i.e. micro air vehicles (MAV). The flight regime in this range of Reynolds number is characterized by transition in combination with laminar separation bubble (LSB). According to Radespiel et al. [1], this transition process is divided into three stages. At the first stage, the primary instability mechanism is of the Tollmien-Schlichting (TS) type. The unstable waves generated by the free stream turbulence or acoustic wave grow exponentially while traveling downstream. At the second stage, the Kelvin-Helmholtz instability may take place. This stage is characterized by nonlinear interactions in which the distortions become so large that saturation occurs and secondary instabilities grow. Finally, the ordered laminar flows break down to turbulence with a rapid increase in the spatial and temporal modes. Additionally, it should be noted that this transition process is strongly influenced by the free stream turbulence level [2].

The size of the laminar separation bubble decreases and the transition occurs early with the increase in the turbulence level. OL [3] performed a series of experiments on the stationary SD7003 airfoil using three different facilities: a low turbulence wind tunnel, a water tunnel and a tow tank. Radespiel et al. [1] conducted experiments on flows past an SD7003 airfoil with and without plunging motion. OL [4] experimentally studied the vortical structures of flow past an SD7003 airfoil with high frequency pitching and plunging. In their experiments, a parameter space of Re and reduced frequency was briefly explored. Recently, Hain et al. [5] studied the dynamics of laminar separation bubbles by using the high-resolution time-resolved particle image velocimetry (TR-PIV) system.

As to the numerical studies, although the direct numerical simulation is a good choice for basic research on this transition phenomenon, it is inapplicable to aerodynamic

---

*Corresponding author (email: hgw@lnm.imech.ac.cn)
† Contributed by HE GuoWei

design due to the speed of current computers. In industrial applications, the Reynolds averaged Navier-Stokes equations (RANS) simulation is widely used. Windte et al. [6] used the RANS to simulate the flows around a stationary SD7003 airfoil. Lian and Shyy [7] used the RANS method coupled with a transition model to tackle flexible airfoil simulation. However, the results from RANS simulation are dependent on the turbulence model and the transition models. And the transition process is often artificially triggered by a pointwise input of turbulent energy. Large-eddy simulation (LES) can capture the unsteadiness of the flows and its results depend less on the subgrid-scale (SGS) model. LES is a good choice for the flapping airfoil simulations in which the unsteady aerodynamics are important. Yuan et al. [8] used a quasi-three-dimensional (only four grids are distributed in the spanwise direction) LES to capture the transition process, without any transition model, for the flows around a stationary SD7003 airfoil. They also tested the effects of the SGS models, including the classical Smagorinsky SGS model, the selective mixed-scale model [9] and an implicit SGS model. His results showed that no appreciable difference was found between the results from the Smagorinsky SGS model and those from the selective mixed-scale model.

Another challenge in the simulation is the moving boundary. The IB method exhibits its advantages to handle the complex geometries and moving boundaries. We refer readers to Peskin [10] and Mittal and Iaccarino's papers [11] for the comprehensive reviews on the IB method. Among the variants of IB methods, the direct forcing method is exclusively designed to handle rigid boundaries. However, it is found in Uhlmann [12,13] that this method introduces non-physical oscillations to the temporal variations of the hydrodynamic force. Yang et al. [14] found that the non-physical oscillations are mainly dependent on the discrete delta functions that are used in the interpolation. Some smoothed discrete delta functions were constructed from the regular discrete delta functions by using a smoothing technique. By using these smoothed discrete Delta functions, the non-physical oscillations can be effectively reduced. The IB method using smoothed discrete delta functions has been successfully applied to laminar flows with stationary and moving boundaries. But its performance in turbulent flows and transitional flows is unknown.

The objective of the present work is to validate the ability of the IB method using the smoothed discrete delta function in simulating transitional flows past moving airfoils including the effect of the IB treatment in the prediction of transition and the smoothing effect of the smoothed discrete delta function at a relatively high Reynolds number.

2 Numerical method

The direct forcing IB method combined with DNS and LES is used in the present work. The central idea of the IB method is to represent the effect of immersed bodies on flows by a virtual volume force. In the present study, the governing equations are the filtered Navier-Stokes equations (with a volume force in the momentum equation):

$$\frac{\partial \overline{u}_i}{\partial t} + \frac{\partial \overline{u}_i \overline{u}_j}{\partial x_j} = -\frac{\partial \overline{p}}{\partial x_i} + \frac{1}{Re}\frac{\partial^2 \overline{u}_i}{\partial x_j \partial x_j} - \frac{\partial q_{ij}}{\partial x_j} + f_i, \quad (1)$$

$$\frac{\partial \overline{u}_i}{\partial x_i} = 0, \quad (2)$$

where x_1, x_2 and x_3 (or x, y, and z) are corresponding to streamwise, cross-wise and spanwise directions respectively, Re is the Reynolds number and f is the volume force. $\overline{u}_1(\overline{u})$, $\overline{u}_2(\overline{v})$ and $\overline{u}_3(\overline{w})$ are the filtered velocity components in the x, y and z directions, respectively. Here q_{ij} is defined as

$$q_{ij} = \tau_{ij} - \frac{1}{3}\tau_{kk}\delta_{ij}, \quad (3)$$

and

$$\tau_{ij} = \overline{u_i u_j} - \overline{u}_i \overline{u}_j, \quad (4)$$

which represents the subgrid-scale stress tensor. The trace of the subgrid-scale stress tensor is lumped together with the pressure.

In the present work, an eddy-viscosity model is used to model q_{ij}. The model is

$$q_{ij} = -2v_t \overline{S}_{ij}, \quad (5)$$

where

$$v_t = C_s^2 \overline{\Delta}^2 \sqrt{2\overline{S}_{ij}\overline{S}_{ij}}, \quad (6)$$

where $\overline{S}_{ij} = \frac{1}{2}\left(\frac{\partial \overline{u}_i}{\partial x_j} + \frac{\partial \overline{u}_j}{\partial x_i}\right)$ is the strain rate tensor. In this model, C_s is the Smagorinsky constant, which has to be determined. In the present work, we simply use C_s=0.1. As proposed by Moin and Kim [15], $\overline{\Delta}$ is multiplied by the Van Driest exponential damping function to account for the reduction in length scales when a solid wall is approached. The Van Driest damping function f_D is defined as

$$f_D = 1 - \exp(-y^+ / A^+), \quad (7)$$

with A^+=25. Here y denotes the minimum distance between the Eulerian grid points and the body surface, which is represented by the Lagrangian markers. In general, y is normalized as $y^+=yu_\tau/v$. Since it is difficult to calculate the friction force in the present IB method, the wall-normal distance y is approximately normalized as

$$y^+ = y\sqrt{F_\tau / \rho}\big/v, \quad (8)$$

where F_τ is the Lagrange force in the wall-tangent direction.

In the present method, the boundary of the immersed body is represented by a series of Lagrangian markers,

while the flow is solved on a set of fixed Cartesian grids. A discrete delta function is used to transfer the quantities between Eulerian and Lagrangian locations. For the simulation of flows past stationary airfoils, a 2-point hat function

$$\phi_2(r) = \begin{cases} 1-|r|, & |r| \leqslant 1, \\ 0, & 1 \leqslant |r| \end{cases} \tag{9}$$

is used without any modification. For the simulations of flows past plunging foil and fully developed turbulent channel flows, one smoothed discrete delta function in Yang et al. [14] is used. This smoothed discrete delta function is then used in the interpolation to reduce force oscillations for the plunging airfoil simulations. The regular discrete delta function is [16]

$$\phi_3(r) = \begin{cases} \dfrac{1}{3}\left(1+\sqrt{-3r^2+1}\right), & |r| \leqslant 0.5, \\ \dfrac{1}{6}\left(5-3|r|-\sqrt{-3(1-|r|)^2+1}\right), & 0.5 \leqslant |r| \leqslant 1.5, \\ 0, & 1.5 \leqslant |r|. \end{cases} \tag{10}$$

The smoothing technique can be expressed as

$$\phi^*(r) = \int_{r-1/2}^{r+1/2} \phi(r')\mathrm{d}r', \tag{11}$$

where ϕ denotes the regular discrete delta function and ϕ^* is the smoothed one. The formulations for ϕ_3^* is shown as follows:

$$\phi_3^*(r) = \begin{cases} \dfrac{17}{48}+\dfrac{\sqrt{3}\pi}{108}+\dfrac{|r|}{4}-\dfrac{r^2}{4}+\dfrac{1-2|r|}{16}\sqrt{-12r^2+12|r|+1}-\dfrac{\sqrt{3}}{12}\arcsin\left(\dfrac{\sqrt{3}}{2}(2|r|-1)\right), & |r| \leqslant 1, \\ \dfrac{55}{48}+\dfrac{\sqrt{3}\pi}{108}+\dfrac{13|r|}{12}+\dfrac{r^2}{4}+\dfrac{2|r|-3}{48}\sqrt{-12r^2+36|r|-23}+\dfrac{\sqrt{3}}{36}\arcsin\left(\dfrac{\sqrt{3}}{2}(2|r|-3)\right), & 1 \leqslant |r| \leqslant 2, \\ 0, & 2 \leqslant |r|. \end{cases} \tag{12}$$

The implementation of the direct forcing IB method in the present work is similar to that in [13]. It can be summarized as the following four steps:

(1) Compute the explicit velocity estimation $\bar{u}$ without volume forces:

$$\tilde{u}_i(\boldsymbol{x},t^{n+1/2}) = u_i(\boldsymbol{x},t^n) + \Delta t\, rhs_i(x,t^{n+1/2}). \tag{13}$$

(2) Calculate the volume forces using the direct forcing method at the Lagrangian locations:

$$F_i(\boldsymbol{X}^{n+1},t^{n+1/2}) = \frac{V_i(\boldsymbol{X}^{n+1},t^{n+1}) - \tilde{U}_i(\boldsymbol{X}^{n+1},t^{n+1/2})}{\Delta t}, \tag{14}$$

where V_i is the velocity of the immersed boundary and it is zero when the boundary is stationary. $\tilde{U}_i$ is a velocity at the Largrangian markers that is interpolated from its Eulerian counterpart $\tilde{u}_i$ by

$$\tilde{U}_i(\boldsymbol{X}^{n+1},t^{n+1/2}) = \sum_{\boldsymbol{x} \in g_h} \tilde{u}_i(\boldsymbol{x},t^{n+1/2})\delta_h(\boldsymbol{x}-\boldsymbol{X}^{n+1})h^3. \tag{15}$$

Here the upper-case letters denote the quantities evaluated at the Lagrangian locations.

(3) Spread the forces at the Lagragian markers to the surrounding Eulerian locations through the discrete delta functions by using the following equation

$$f_i(\boldsymbol{x},t^{n+1/2}) = \sum_{l=1}^{N_l} F_i(\boldsymbol{X}_l^{n+1},t^{n+1/2})\delta_h(\boldsymbol{x}-\boldsymbol{X}_l^{n+1})\Delta V_l, \tag{16}$$

where ΔV_l is the volume of the lth Lagrangian grid.

(4) Solve the Navier-Stokes equations on the Cartesian grid with the volume forces.

The spatial discretization scheme is based on a second order finite volume formulation on a staggered mesh. The governing equations are advanced in time using the fractional step method. The third order Runge-Kutta scheme is used for the terms that are treated explicitly and the Crank-Nicholson scheme is used for the terms that are treated implicitly.

3   Results and discussion

3.1   Fully developed turbulent channel flows

A direct numerical simulation of the fully developed turbulent channel flows is performed using the direct forcing IB method. The Reynolds number based on the friction velocity and the half channel width is 180. The computation domain is $4\pi h \times \dfrac{4}{3}\pi h \times 2h$, where h is the half channel width.

The total grid number is 128×166×128 in the streamwise, wall-normal and spanwise direction, respectively. The meshes in the streamwise and spanwise directions are uniform, while the meshes in the wall normal direction are non-uniform with the grid clustering near the solid walls. The mesh is coincident with the upper wall so that the no-slip boundary condition can be imposed on the upper wall exactly. However, near the lower wall the grid is artificially distributed that the grid does not coincide with the wall for all velocity components. The IB method is used on the lower wall to satisfy the no-slip boundary conditions. In this setup, the utilization of the IB method is more likely to affect the prediction of the velocity profile in the lower half of the channel while the influence on the velocity profile in the upper half is relatively small.

The upper plot in Figure 1 compares the mean velocity profile of the lower half channel with the one in the upper half channel. They are in good agreement and only some minor differences are found at $y^+<5$. It is observed from the lower plot in Figure 1 that the rool-mean-square (r.m.s.). velocity fluctuations in the lower half channel are in good agreement with the ones of the upper half channel. Thus, in terms of the first-order and second-order turbulent statistics, the direct forcing IB method with the 4-point function ϕ_3^* in simulating fully developed turbulent channel flow is validated.

3.2 Transitional flows past an airfoil

In this section, the results of transitional flows past a stationary/plunging SD7003 airfoil are presented. The Reynolds number based on the chord length C and the inflow velocity U_∞ is 60000. The angle of attack α is 4° for both the stationary case and the plunging case.

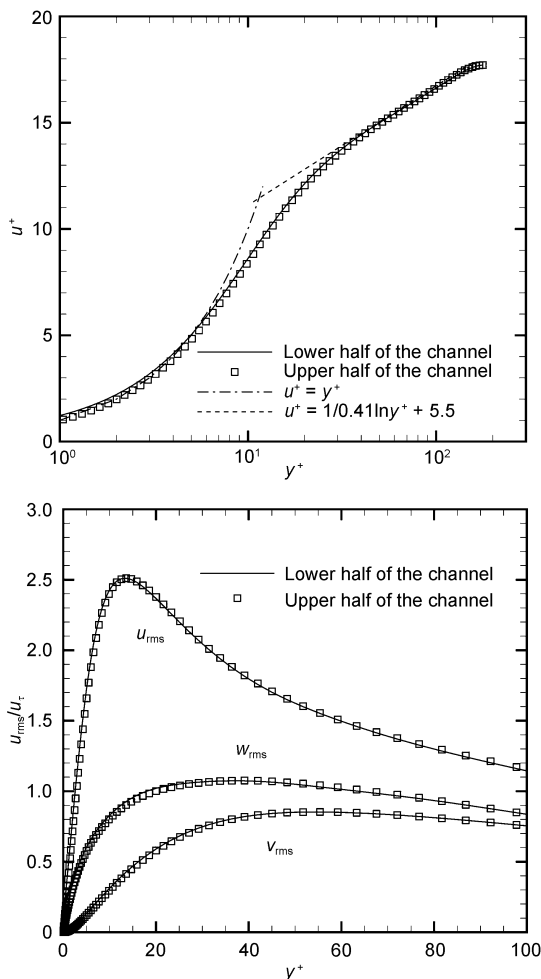The dimensions of the computational domain are $10C$,

Figure 1 Time and spanwise averaged mean velocity profiles and r.m.s. velocity fluctuations for fully developed turbulent channel flows at *Re*=180 with the lower wall that is not coincident with the grids. Upper plot: mean velocity profile. Lower plot: r.m.s. velocity fluctuations.

$6C$, and $0.5C$ in the streamwise (x_1), wall normal (x_2) and spanwise (x_3) directions, respectively.

The boundary conditions are given as follows: at the inlet, a uniform flow with the speed U_0 is specified; at the outlet, a convection velocity boundary condition is applied; at the crosswise boundaries, the shear-free boundary condition is specified on the velocity. A periodic boundary condition is specified in the spanwise direction. The mesh size is uniform near the airfoil and the mesh is stretched to a larger size in the far field. For the stationary case, the total grid number is 913×278×32 with the minimal mesh size being $0.0025C$. For the plunging case, the total grid number is 561×252×32 with the minimal mesh size being $0.005C$. Figure 2 plots the Cartesian grid used for the stationary case. Only at the first time step, random forces with amplitude 10^{-8} are applied on the airfoil surface in the spanwise direction in order to develop the transitional flows quickly. Note that the transition can occur without applying these random forces.

In the IB method, the hydrodynamic stress on the surface can not be calculated directly since the Cartesian grid does not coincide with the immersed boundary in general. As shown in Figure 3, the velocity and the pressure at point B are averaged from the surrounding fluid points. The friction force at the Lagrangian point A is then constructed by using one side difference. The pressure at Lagrangian point A is
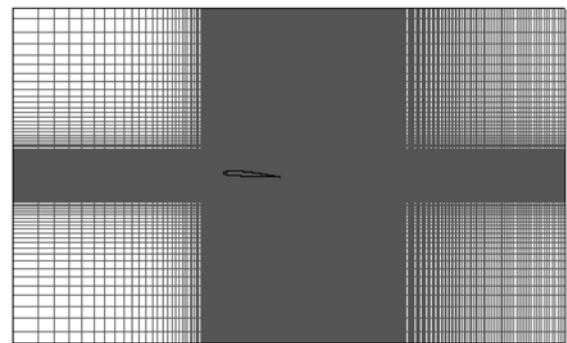

Figure 2 Cartesian grid for the simulation of flows past a stationary airfoil.
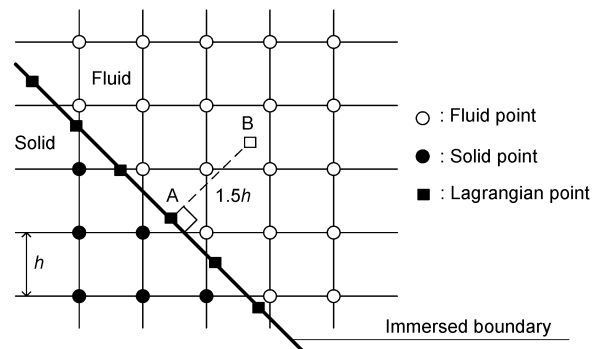

Figure 3 A schematic display of the pressure and friction calculation at the Lagrangian points.

equal to the pressure at point B by using the boundary condition of pressure $\partial p / \partial n |_{wall} = 0$.

The temporal variations of the drag and the lift are evaluated as the summation of the volume force as in eq. (14) in the streamwise and crosswise directions, respectively. For the problems with moving boundaries, the inertial force of the "pseudo fluid" enclosed by the immersed boundary needs to be subtracted. Please refer to paper [12] for the details of the hydrodynamic force calculation.

3.2.1   Flows past a stationary airfoil

In the near wall region especially near the leading edge, the grid is too coarse to resolve the thin laminar boundary layer, so we can not expect to accurately capture the friction and the pressure around the leading edge. The upper plot of Figure 4 shows the time-averaged pressure coefficient on the surface of airfoils. Near the leading edge, the boundary layer separates from the surface caused by a strong adverse pressure gradient. After the separation, a pressure plateau appears which corresponds to the laminar separation bubble. The pressure plateau terminates at the transition point where
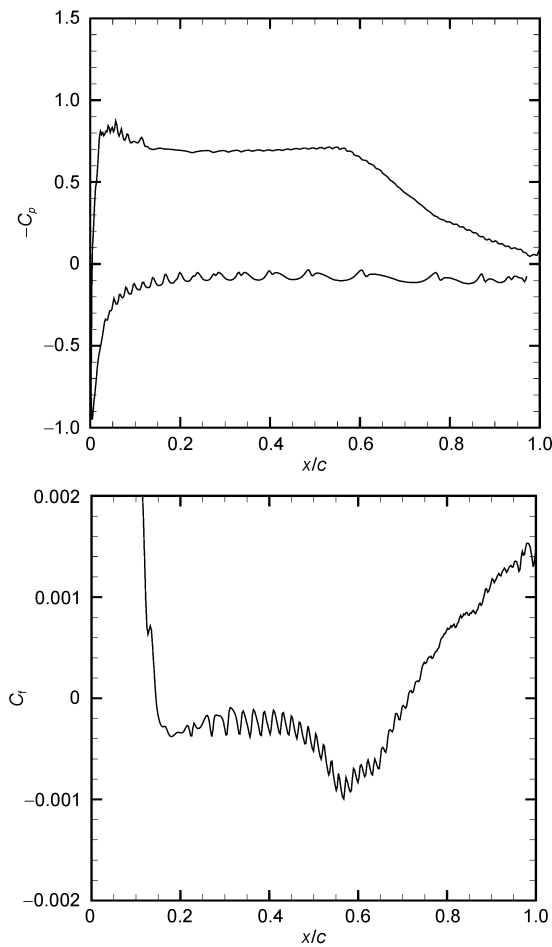
the transition of the shear layer causes a rapid increase in the surface pressure. After a complete transition to turbulence, the flows show reattachment due to the large turbulence momentum transport towards the airfoil surface.

The time-averaged friction coefficient is shown in the lower plot of Figure 4. The friction coefficient is negative between x/c=0.16 and 0.71 which is related to the laminar separation bubble. And the points x/c=0.16 and x/c=0.71 are the separation point and reattachment point, respectively. After the reattachment, the friction coefficient shows an increase due to the turbulent flows. The separation point, transition point and reattachment point of the present simulations compared with the ones from numerical simulations and experiments in other references are shown Table 1. The separation point and reattachment point are determined from the distribution of friction coefficient as shown in the lower plot in Figure 4. As to the transition, there are various ways to determine its location, such as intermittency methods [17] and fluctuation growth methods [18]. In the present study, the commonly used Reynolds-stress threshold method is adopted. In this method, the transition point is defined as the beginning of the turbulent wedge that spreads from the shear layer of the LSB. Usually the point is taken where the normalized Reynolds shear stress is −0.001 and its amplitude demonstrates a clearly visible rise as is the case in other studies [19,1]. In the present study, the threshold of Reynolds stress is taken as −0.005 rather than −0.001. By using this threshold, the transition point is 0.45. If the threshold is taken as −0.001, the transition point is 0.3. But at x/c=0.3, the amplitude of the Reynolds stress does not show a clear increase, so we take x/c=0.45 as the transition point in the present study. The transition point and reattachment point obtained are consistent with those in the literature [19,1]. However, the separation appears to occur earlier compared the numerical results in the literature. The possible reason for the earlier separation is the lack of mesh resolution near the leading edge in the present study.

The Reynolds shear stress distribution and the time-averaged streamlines on the suction surface of the airfoil are shown in Figure 5. As shown in the plot, the Reynolds stress is near zero in the first half of the LSB. After the transition point x/c=0.45, the amplitude of Reynolds stress shows a visible increase along the shear layer. The maximum location of the amplitude of the Reynolds stress is just on the top of the rear part of the LSB. These phenomena show good agreement with Radespiel et al.'s experiment [1], although the separation bubble is larger and longer than that

Figure 4   Spanwise- and time-averaged pressure coefficient and friction coefficient on the airfoil surface at *Re*=60000 and α=4°. Upper plot: pressure coefficient. Lower plot: friction coefficient.

Table 1   The separating point, transition point and reattaching point for flows past a stationary SD7003 airfoil at *Re*=60000 and α=4°

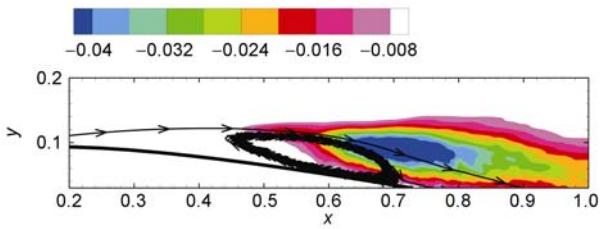|	x_s/c	x_t/c	x_r/c
Present results	0.16	0.45	0.71
LES 3D by Yuan et al. [19]	0.25	0.49	0.60
Exp. by Radespiel et al. [1]		0.55	0.64

Figure 5 The iso-contours of turbulent shear stress $\overline{u'v'}$ and time-averaged streamlines for the flows past a stationary SD7003 airfoil at $Re=$ 60000 and $\alpha=4°$.

in the experiment. The relatively large size of the LSB is probably caused by two reasons. The first is the zero level of the free stream turbulence. The second reason is the early separation of the laminar boundary layer.

Figure 6 plots the instantaneous iso-surface of spanwise vorticity. The plots show that in the first half of the chord length, the flow structure is two-dimensional. Nearly in the middle of the airfoil, the two-dimensional structure is distorted and abruptly the two-dimensional structures break down to small three-dimensional structures. With the interaction of the vortex with the surface of the airfoil, even small structures are generated. The flows reattach on the airfoil surface. It should be noted that the transition point is not given *a priori*. The development of three-dimensional turbulent structures is triggered solely by the numerical noises.

The method has demonstrated its use in simulating transitional flows with stationary boundaries in particular the capture of the three-dimensional flow. The results for the plunging airfoil simulations will be presented in the next section.

3.2.2　*Flows past a plunging airfoil*

In this subsection, we present the numerical results of the flows past a plunging airfoil. The plunging motion of the airfoil is prescribed as

$$y(t) = A\cos(2\pi f t), \qquad (17)$$

where the amplitude is $A=0.05C$ and the reduced frequency k, defined as $k = \pi f C / U_\infty$, is 3.93. The amplitude and the reduced frequency used in this study are the same as those in the experiment [4].
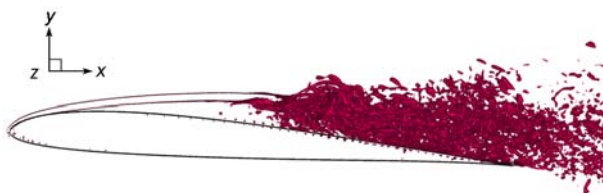

Figure 6 Instantaneous iso-surface of the spanwise vorticity ($\omega_z=-40$) for the flows past a stationary SD7003 airfoil at $Re=60000$ and $\alpha=4°$.

The iso-contours of the phase- and spanwise-averaged spanwise vorticity at four different phases are shown in Figure 7. The figure shows that two vortices with opposite signs are shedding from the trailing edge within one cycle. The positive one is generated when the airfoil plunges down from the position with zero displacement (downstroke, $\alpha=1/4$), while the negative one is from the upstroke ($\phi=3/4$). In the wake, an inverse Karmann vortex street has formed.

Moreover, the vortex shed during the downstroke has a higher intensity than the one shed during the upstroke. By measuring the displacement of one vortex motion in one
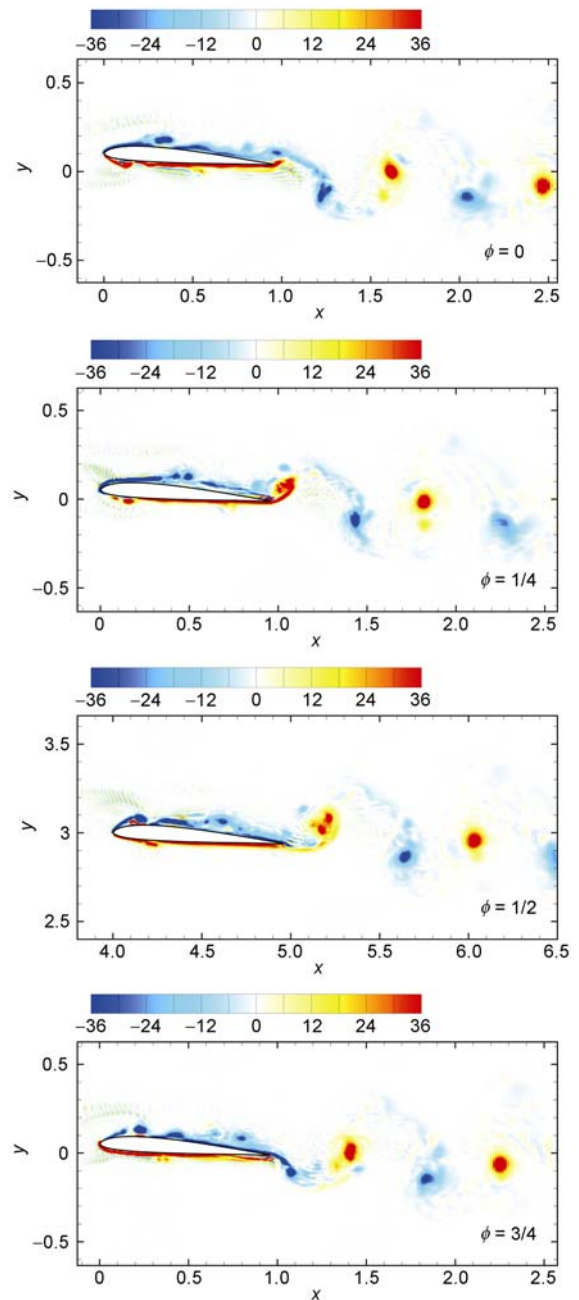

Figure 7 Phase- and spanwise-averaged spanwise vorticity contours for flows past a plunging SD7003 airfoil at $Re=60000$ and $k=3.93$.

cycle, it can be seen that the vortex moves downstream nearly at the free-stream velocity. All of these observations are in good agreement with the experiment in [4].

Figure 8 shows the iso-contours of the phase and spanwise averaged turbulent kinetic energy at four different phases. These two pictures show that the locations of high turbulent kinetic energy in the wake are coincident with the cores of the spanwise vortices. Besides that in the wake, the turbulent kinetic energy is mainly distributed near the surface of the airfoil, especially on the upper surface of the airfoil. The turbulence on the surface is probably generated within the shear layer separated from the wall which is the
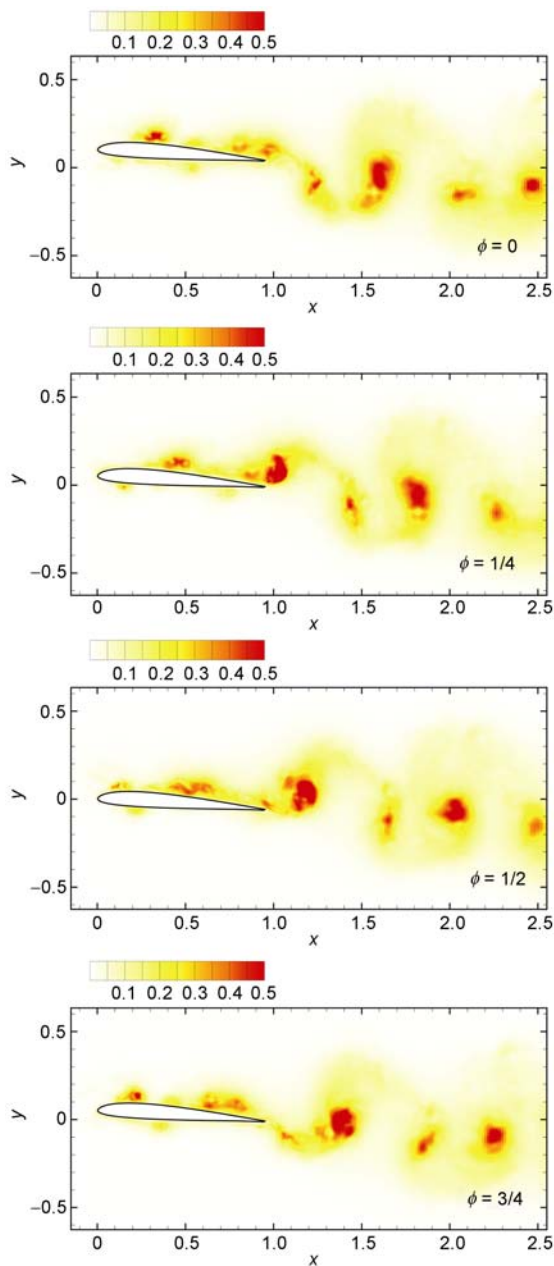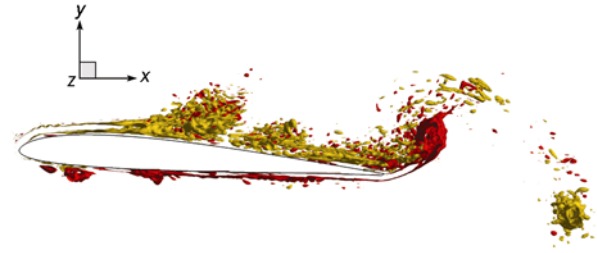

Figure 9   Instantaneous iso-surface of the spanwise vorticity for flows past a plunging SD7003 airfoil at *Re*=60000 and *k*=3.93. Red iso-surface: ω_z=40; yellow iso-surface: ω_z=−40.

same as the stationary case. The sources for the turbulent fluctuations in the wake are complicated. Some turbulent fluctuations are from the upstream, and the others may be generated by the stirring effect of plunging motion at the trailing edge.

Figure 9 shows an instantaneous three-dimensional iso-surface of the spanwise vorticity. On the suction surface, the flow structure is two-dimensional near the leading edge,
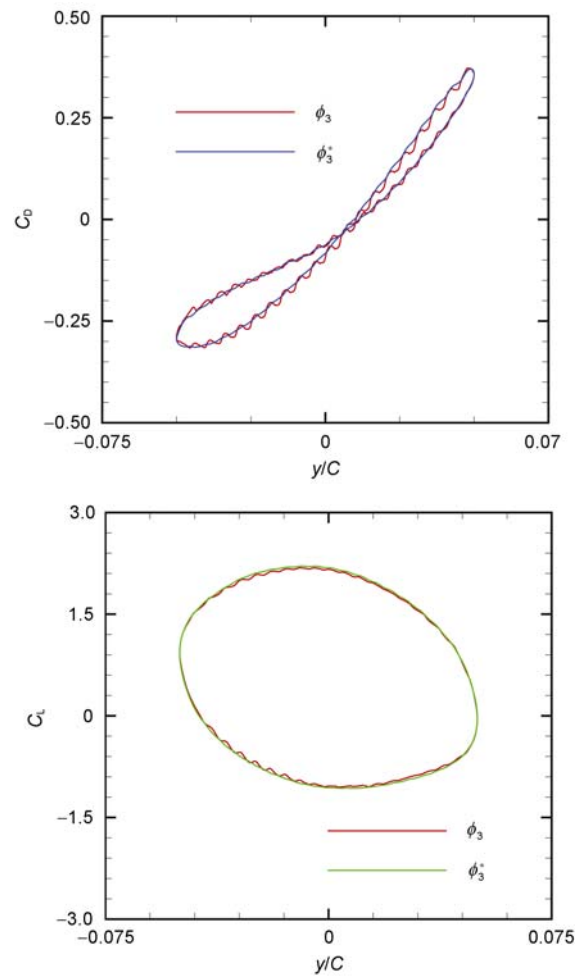

Figure 8   Phase- and spanwise-averaged turbulent kinetic energy contours for flows past a plunging SD7003 airfoil at *Re*=60000 and *k*=3.93.

Figure 10   Periodic-variations of the drag coefficient and the lift coefficient for flows past a plunging SD7003 airfoil at *Re*=60000 and *k*=3.93. Upper plot: drag coefficient; lower plot: lift coefficient.

then it is distorted, and finally it breaks down to small three-dimensional structures. The evolution of the flow structure on the suction surface is similar to that in the stationary case, but the breakdown to three-dimensional structures happens earlier in the plunging case. On the pressure surface, spanwise vortices exist which are absent in the stationary case.

Figure 10 compares periodic-variations of the drag coefficient and lift coefficient obtained from the regular 3-point function ϕ_3 and the ones obtained from the smoothed 3-point function ϕ_3^* for the plunging airfoil simulations. For the results from ϕ_3, especially on the drag coefficient, small wiggles exist on the hydrodynamic forces for this plunging case, while for the results from ϕ_3^*, the non-physical oscillations are effectively suppressed and smooth periodic-variations are obtained.

4   Conclusions

The IB method has exhibited its advantage in simulating laminar flows with complex or moving boundaries. To test its validity in turbulent flows, we first simulate a fully developed turbulent channel flow using DNS combined with the IB method. The results obtained are in good agreement with those of DNS using a body-fitted grid. Furthermore, we simulate the transitional flows around the stationary and plunging airfoils at Re=60000 using LES combined with the IB method. The results are consistent with those from experiments. For the stationary case, the IB method makes good predictions of the location of transition and reattachment. For the plunging case, the vortex structures are also in good agreement with experimental results. In both the stationary and plunging cases, the three-dimensional flow structures are well captured. By using a smoothing technique, the non-physical oscillations in hydrodynamic forces are successfully suppressed and the smooth temporal variations are obtained. The capability of the present method in simulating turbulent and transitional flows is demonstrated through the above numerical simulations.

The present work suggests that LES with the direct forcing IB method could be used to simulate the flows around the flapping airfoils at moderate Reynolds numbers. To obtain more accurate predictions requires more refined grids. In the present IB method, the refinement has to be done in all the three directions and the grids in the far field are unnecessarily refined. This causes a large increase in the total grid number. One possible solution to this issue is to use the local refinement in regions where the immersed boundaries are located. The other possible solution is to appropriately model the shear layer separation, turbulent transition and reattachment. As the first step in future work, we will develop the wall-layer models for the present LES with the direct forcing IB method.

1   Radespial R, Windte J, Scholz U. Numerical and experimental flow analysis of moving airfoils with laminar separation bubbles. In: 44th AIAA Aerospace Sciences Meeting and Exhibit, 9-12 January 2006, Reno, Nevada. AIAA paper, 2006, AIAA-2006-501

2   Wissink J, Rodi W. DNS of a Laminar Separation Bubble Affected by Free-stream Disturbances. Dordrecht: Springer/Kluwer Academic, 2004

3   OL M V, McAuliffe B R, Hanff E S, et al. Comparison of laminar separation bubble measurement on a low Reynolds number airfoil in three facilities. In: 35th AIAA Fluid Dynamics Conference and Exhibit, Toronto, Ontario Canada. AIAA Paper, 2005, AIAA-2005-5149

4   OL M V. Vortical structures in high frequency pitch and plunge at low Reynolds number. In: 37th AIAA Fluid Dynamics Conference and Exhibit, 25-28 June 2007, Miami, FL. AIAA Paper, 2007, AIAA-2007-4233

5   Hain R, Kähler C J, Radespiel R. Dynamics of laminar separation bubbles at low-Reynolds-number airfoils. J Fluid Mech, 2009, 630: 129–153

6   Windte J, Scholz U, Radepiel R. Validation of the RANS simulation of lamonar separation bubbles on airfoils. Aerosp Sci technol, 2006,10: 484–494

7   Lian Y, Shyy W. Laminar-turbulent transition of low Reynolds number rigid or flexible airfoil. AIAA J, 2007, 45: 1501–1513

8   Yuan W, Xu H, Khalid M, Radespiel R. A parametric study of LES on laminar-turbulent transitional flows past an airfoil. Int J Comp Fluid Dyn, 2006, 20: 45–54

9   Lenormand E, Sagaut P, Phuoc L, et al. Subgrid-scale models for large-eddy-simulation of compressible wall bounded flows. AIAA J, 2000, 38: 1340–1350

10   Peskin C S. The immersed boundary method. Acta Numer, 2002, 11: 479–517

11   Mittal R, Iaccarino G. Immersed boundary methods, Annu Rev Fluid Mech, 2005, 37: 239–261

12   Uhlmann M. First experiments with the simulation of particulate flows. Technical Report, No.1020, CIEMAT, Madrid, Spain, ISSN 1135-9420, 2003

13   Uhlmann M. An immersed boundary method with direct forcing for the simulation of particulate flows. J Comput Phys, 2005, 209: 448–476

14   Yang X, Zhang X, Li Z, He G W. A smoothing technique for discrete delta functions with application to immersed boundary method in moving boundary simulations. J Comput Phys, 2009, 228: 7821–7836

15   Moin P, Kim J. Numerical investigation of turbulent channel flow. J Fluid Mech, 1982, 118: 341–371

16   Roma A M, Peskin C S, and Berger M J. An adaptive version of the immersed boundary method. J Comput Phys, 1999, 153: 509–534

17   Roberts S K, Yaras M I. Effects of periodic unsteadiness, freestream turbulence and flow Reynolds number on separation-bubble transition. ASME paper No. GT2003-38626, 2003

18   McAuliffe B R, Yaras M I. Separation-bubble-transition measurements on a low-Re airfoil using particle image velocimetry. ASME paper No. GT2005-68663, 2005

19   Yuan W, Khalid M. An investigation of low-Reynolds-number flows past airfoils. In: 23rd AIAA Aerodynamics conference Toronto. AIAA Paper, 2005, AIAA-2005-4607